Colloids and Surfaces A: Physicochemical and Engineering Aspects 642 (2022) 128626

Contents lists available at ScienceDirect

Colloids and Surfaces A: Physicochemical and Engineering Aspects

journal homepage: www.elsevier.com/locate/colsurfa

A comparative study of chemical treatment by $MgCl_2$, $ZnSO_4$, $ZnCl_2$, and KOH on physicochemical properties and acetaminophen adsorption performance of biobased porous materials from tree bark residues

Glaydson S. dos Reis [a,*], Marine Guy [b], Manon Mathieu [c], Mohamed Jebrane [d], Eder C. Lima [e], Mikael Thyrel [a], Guilherme L. Dotto [f], Sylvia H. Larsson [a]

[a] Department of Forest Biomaterials and Technology, Swedish University of Agricultural Sciences, Biomass Technology Centre, SE-901 83 Umeå, Sweden
[b] Chimie ParisTech – PSL, Paris, France
[c] IMT Mines Albi-Carmaux, Albi, France
[d] Department of Forest Biomaterials and Technology, Swedish University of Agricultural Sciences, Vallvägen 9C, 750 07 Uppsala, Sweden
[e] Institute of Chemistry, Federal University of Rio Grande do Sul (UFRGS), Av. Bento Gonçalves 9500, Porto 13 Alegre 91501-970, Brazil
[f] Chemical Engineering Department, Federal University of Santa Maria (UFSM), Santa Maria 97105-900, RS, Brazil

HIGHLIGHTS

- Porous carbons were prepared by simple methods using $MgCl_2$, $ZnSO_4$, $ZnCl_2$, and KOH.
- KOH activation yielded a porous carbon with a specific surface area of 2209 m^2 g^{-1}.
- Compared to other chemicals, $MgCl_2$ yielded an extremely hydrophobic material.
- Ultrafast acetaminophen adsorption times were reached for all activation methods.
- Regeneration studies showed good cyclability at around 70% in the 3rd cycle.

GRAPHICAL ABSTRACT

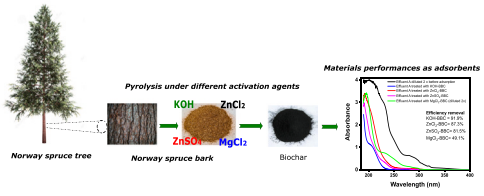

ARTICLE INFO

Keywords:
Norway spruce bark
Bio-based carbon porous materials
Different chemical activation
Ultrafast acetaminophen removal
Pore-filling mechanism of adsorption

ABSTRACT

Preparing sustainable and highly efficient biomass-based carbon materials (BBPM) as adsorbents remains a challenge for organic pollutant management. In this work, novel biobased carbon material has been synthesized via facile, sustainable, and different single-step pyrolysis chemical methods (KOH, $ZnCl_2$, $ZnSO_4$, and $MgCl_2$) using a Norway spruce bark as suitable and efficient carbon precursor. The effects of each chemical activator on the physicochemical structure of synthesized were thoroughly investigated as well as its performance on the acetaminophen adsorption. The results showed that the use of different chemical activation provoked remarkable differences in the BBPM physicochemical characteristics. The KOH activation generated material with the highest specific surface area (2209 m^2 g^{-1}), followed by $ZnCl_2$ (1019 m^2 g^{-1}), $ZnSO_4$ (446 m^2 g^{-1}), and $MgCl_2$ (98 m^2 g^{-1}). The chemical characterization of the carbon materials indicated that the activation of $MgCl_2$ yielded a material around three times more hydrophobic when compared with the other activation methods. The acetaminophen removal showed to be ultrafast, not only due to the BBPM's microstructure but also to the

* Corresponding author.
E-mail addresses: glaydson.simoes.dos.reis@slu.se, glaydsonambiental@gmail.com (G.S. dos Reis).

https://doi.org/10.1016/j.colsurfa.2022.128626
Received 24 December 2021; Received in revised form 8 February 2022; Accepted 20 February 2022
Available online 25 February 2022

abundant active sites provided by the different chemical activation methods. The adsorption equilibrium times were reached at 1 min for BBPM-KOH and BBPM-$MgCl_2$ and 15 min for BBPM-$ZnSO_4$ and BBPM-$ZnCl_2$. The adsorption process suggests that the pore-filling mechanism mainly dominates the acetaminophen removal but also some physical-chemical interactions such as hydrogen bonding between the amide group of acetaminophen and oxygenated or nitrogenated groups of biochar, π-π interactions between the aromatic ring of the pharmaceutical and the aromatics of biochar, n-π interaction, van der Waals interactions. The BBPM regeneration studies showed very good cyclability; in the 3rd cycle, the removal was approximately 70% for all four samples. The samples were also used to treat two synthetic effluents, which attained a removal percentage up to 91.9%.

1. Introduction

Biomass is a carbon source that can effectively be employed for energy and materials synthesis design as promising and exciting alternatives to fossil sources. One good option for biomass management is applying it as a precursor to producing bio-based carbon porous materials (BBPM) [1–3]. BBPM is defined as a black carbonaceous porous solid material with high specific surface area (SSA), developed porosity, ordered pore size distribution, and rich in functionalities on its surface [1–6]. BBPM is produced from sustainable sources (biomass precursors) through the thermal decomposition of biomass under an inert atmosphere (absence of oxygen) at elevated temperatures [2–8].

The BBPM's properties are severely dependent on the type of biomass precursor and its preparation method [1,2]. The BBPM preparation method consists of two main procedures (i) pyrolysis and (ii) activation [1,2]. The main goal of pyrolysis is to reduce the volatile content of the biomass precursors in the temperature range of 300–900 °C and create a solid structure with primary porosity associated with a high fixed carbon content [2,9]. On the other hand, the main idea behind the activation process is to develop and maximize the primary porosity to enhance the SSA and pore volume structure of BBPM through opening new pores and widening the existing ones [9–11]. In addition, the activation process can vary and/or adjust the chemical surface of the biobased material to tailored, unique characteristics [9,10]. Therefore, the activation process is considered more influential than carbonization in terms of the properties of the BBPM.

The most usual activating agents used are KOH, NaOH, $ZnCl_2$, Na_2CO_3, and H_3PO_4 [12]. However, $ZnSO_4$, $AlCl_3$, and $MgCl_2$ can also be an alternative [13,14]. The type of chemical activator employed will influence the action mechanism and the chosen pyrolysis temperatures for efficient activation of the carbon-based material. The activation mechanism of KOH is based on solid-solid or solid-liquid reactions involving hydroxide reduction and carbon oxidation. The CO and H_2 are considered subproducts, while the interaction mechanism with ZnCl2 is based on the catalytic dehydration with the ZnCl2 acting as a skeleton during carbonization, with positive effects on pore structure-specific surface area [11,14].

The chemical activators dehydrate, oxidize, or break down the biomass raw material, and during the pyrolysis, the carbon skeleton is charred and aromatized, which further leaches out step, materials with highly porous structure can be generated [12–14]. In addition, chemical activation delays the burning of precursor materials, favoring higher product yield [13,14]. Therefore, the chemical activation process, when compared to physical activation, has several advantages such as (i) shorter pyrolysis time and short pyrolysis temperature, leading to low energy consumption being economical from the energy viewpoint, (ii) minimization of elimination of volatile organic compounds leading to higher carbon yields, (iii) better development of uniform porous structure, (iv) larger surface areas and (v) higher number of functional groups on the pyrolyzed material's surface [12–14].

Together with the chemical activation, the characteristics of the biomass precursor play a vital role in the features of the final pyrolyzed product. BBPM can be produced from a large variety of carbonaceous precursors, and for selecting a suitable precursor, its availability, cost, and main composition should be considered. In this research, Norway spruce bark (*Picea abies* (Karst.) L.) was chosen as an effective carbon source to produce bio-based carbon porous materials. Norway spruce is a common tree that covers a large part of the north of Europe, especially in Scandinavia [15]. Spruce bark is rich in tannins [15], and its main components are lignin, hemicellulose, and cellulose, being suitable for producing BBPMs [16].

The spruce bark bio-based carbon porous materials were utilized as adsorbents to remove acetaminophen (AMP) from aqueous wastewaters. AMP belongs to a class of pharmaceuticals that is considered an emerging contaminant [17,18]. AMP is the most common analgesic and antipyretic pharmaceutical prescribed worldwide, and due to its extensive use, it is commonly found in the environment such as rivers and lakes [17]. Therefore, wastewaters must be adequately treated before being discharged into the environment [18]. Conventional wastewater treatment methods are not wholly efficient in removing pharmaceuticals. Therefore, specific methods such as biological processes [19], filtration techniques [20], oxidation [21,22], photocatalytic degradation [23], and adsorption [7,18,24] are employed. However, these processes are costly and involve high initial investments and operational costs. On the contrary, adsorption is a more attractive method because contaminants are removed, and the adsorbent can be reused several times, making the wastewater treatment process economically feasible.

The current state-of-the-art presents a large gap between our ability to produce different carbon materials from biomasses, using different activation methods, and how their properties are connected to the resulting carbon performances in adsorbing pollutants from waters or performances in other possible applications. This research helps diminish that gap by explicitly focusing on the minute correlation of carbon properties linking its chemical activation method with the resulting material properties. Furthermore, by employing different c Therefore, this research can provide a reasonable understanding of the effect of the different chemical activation methods on the carbon physical-chemical and adsorption features.

The aims of this work comprise (i) the production of BBPMs from Norway spruce bark as a carbon precursor by using four chemical activators ($MgCl_2$, $ZnSO_4$, KOH, $ZnCl_2$); (ii) to study the effect of each chemical activator on the physicochemical and adsorption properties of the BBPM materials; (iii) to apply the BBPM as adsorbents for acetaminophen removal from aqueous solution and to treat synthetic effluents containing several emerging pollutants.

This study permitted to build off an optimized activation methodology that involves understanding the role of each activator ($ZnSO_4$, $MgCl_2$, KOH, and $ZnCl_2$) on the physicochemical features of the biobased porous materials and, later on, their performances on acetaminophen removal from aqueous solution. To the best of our knowledge, there are few investigations on pyrolysis of biomass dealing with $MgCl_2$ and none with $ZnSO_4$, which further justifies this work.

2. Experimental

2.1. Biomass

The tree bark was obtained and treated as described elsewhere [25]. The four chemical reagents ($MgCl_2$, $ZnSO_4$, KOH, $ZnCl_2$) were acquired

from Merck, and distilled water was used throughout the BBPMs preparation.

2.2. BBPM preparation

According to a previously reported procedure, the BBPMs were produced through a single pyrolysis step and activation [5–8,24]. First, 20.0 g of biomass was mixed with the selected chemical reagent, and distilled water was added to the mix until homogenous pastes were obtained [5–8,24,25]. Then, the mixtures were left at an ambient temperature for 2 h before being placed on a stove at 105 °C for 24 h. Once the pyrolysis was completed, the oven was shut down, and the door opened to cool down, still under N_2 flow until a temperature of 200 °C was reached. Then the N_2 flow was stopped until the oven reached the ambient temperature. Afterward, to remove the remaining chemical reagents KOH, $ZnCl_2$, $ZnSO_4$, and $MgCl_2$, and washing step was performed with HCl solutions at concentrations of 1.0 M (for KOH treated materials) [11], 6.0 M ($ZnCl_2$ treated materials) [6,7], 4.0 M ($ZnSO_4$ treated materials) and 2.0 M ($MgCl_2$ treated materials) [13]. Next, the samples were heated at 80 °C for 1 h with these solutions under a reflux system. After that, the samples were filtered and exhaustively washed with distilled water to remove the remaining acid from the BBPM structures until a stable pH was obtained in the filtrate [6,8].

2.3. Batch adsorption and regeneration tests

The acetaminophen initial solution concentrations used for the adsorption tests varied from 70 to 1200 mg L^{-1} at different pH (3.0–9.0). Next, a mass of 30 mg of BBPM samples was added to 20.00 mL acetaminophen aliquant solution in 50.0 mL flat cylindrical tubes. All the adsorption tests were carried out at 23 °C. First, the tubes were shaken in a KS250 shaker (IKA Labortechnik) for 1–180 min. Afterward, to separate the BBPM from the solutions, the tubes were centrifugated for 30 min, and with a pipette, the needed solution was withdrawn. Then, the residual acetaminophen solutions were measured using a UV-Visible spectrophotometer (Shimadzu 1800) at λ_{max} of 244 nm.

The sorption capacity (Eq. 1) and the percentage of acetaminophen removal (Eq. 2) are given below:

$$q = \frac{(C_0 - C_f)}{m}.V \quad (1)$$

$$\%\ \ Removal = 100.\frac{(C_0 - C_f)}{C_0} \quad (2)$$

q is the amount of acetaminophen uptaken by the biochars (mg g^{-1}). C_o and C_f are the initial and final acetaminophen concentrations (mg L^{-1}), respectively. m is the mass of BBPM (g), and V is the aliquant of the acetaminophen solution (L).

For regeneration tests, acetaminophen-laden biochars were washed with water to remove any unadsorbed drug and dried overnight in an oven at 50 °C. The dried-laden biochars were contacted with two eluents, i.e., 0.1 M NaOH + 20% EtOH and 0.25 M NaOH + 20% EtOH and agitated for 6 h. The desorbed pharmaceutical was then separated from the biochar. The latter was washed with water to remove the eluent and dried overnight in an oven at 50 °C. The adsorption capacity of the recycled adsorbent was measured again. A total of four consecutive adsorption-desorption cycles were carried out.

The statistical evaluation of the models is presented in Supplementary Material [6,7,24,26–28].

2.4. Models of kinetics and isotherms of adsorption

The kinetics and equilibrium models are given in Supplementary Material [6,7,26–28].

2.5. Effluent treatment

Two effluents loaded with several drugs and organic/inorganic compounds were made to simulate hospital effluents [7,8]. These synthetic effluents with different compositions (Supplementary Table 1) were prepared to test the BBPM's ability to treat real effluents [7,8].

3. Results and discussion

3.1. Characterization of the biobased porous materials (BBPM) samples

3.1.1. N_2 isotherms and textural properties

N_2 adsorption-desorption isotherms for BBPM-KOH, BBPM-$ZnCl_2$, BBPM-$ZnSO_4$, and BBPM-$MgCl_2$ samples are presented in Fig. 1. The chemical treatment yielded BBPM with different isotherm curves. According to the International Union of Pure and Applied Chemistry (IUPAC) classification [29], the isotherm for BBPM-KOH has its shape closer to type I (with portions of type II and IV); type I is related to microporous materials; however, it shows hysteresis from partial pressure of 0.4 (which related to isotherm type IV), highlighting the presence of mesoporosity [29]. In addition, BBPM-KOH isotherm did not reach a limiting value, and the shape of isotherms at high partial pressure can be related to type II [29]. BBPM-$ZnCl_2$ can be classified as a combination of type I and type II, with a prominence of micropores in its structure [29]. Also, as for BBPM-KOH, the portion at high pressure, the curve did not reach the limiting value, which can be related to type II isotherm. On the other hand, BBPM-$ZnSO_4$ and BBPM-$MgCl_2$ samples show curves closer to type IV (IUPAC) [29], with evident hysteresis, typical of mesoporous materials with pore width between 2 nm and 50 nm.

The differences in the pore structure indicated by the N_2 isotherms are also reflected in the pore size distribution curves (see supplementary Fig S1). For example, BBPM-KOH exhibits large quantities of small mesopores (3.74–4.06 nm) and micropores centered at 1.79 nm, whereas BBPM-$ZnCl_2$ has a sharp peak at 1.74 nm, which signifies a microporous material.

The N_2 isotherms for BBPM-$ZnSO_4$ and BBPM-$MgCl_2$ do not have microporous characteristics (as suggested). The BBPM-$ZnSO_4$ shows a sharp peak at 3.76 nm and fractions of mesopore in the range of 4.5–14.3 nm, while BBPM-$MgCl_2$ presents a peak at 3.84 nm and fractions of big mesopores between 24 and 49 nm (not shown). The difference in the pore size distribution of BBPM samples effectively affects the SSA and thereby the AMP adsorption as the adsorption of a sorbing species partly depends on the pore sizes [6,24,30].

Table 1 shows the Specific Surface Area (SSA), area of micropores (A_{Micro}), and mesopore area (A_{Meso}) of the BBPM samples; as can be seen, the sample activated with KOH exhibited the highest SSA value, followed by $ZnCl_2$, $ZnSO_4$, and $MgCl_2$. Furthermore, the SSA values match with the total amount of adsorbed N_2 (see Fig. 1). Thus, it is clear that the chemical activator significantly influences the textural properties, which can also effectively influence the adsorption properties. Kopac et al. [4] reported that different types of biomass, chemical activation, and pyrolysis conditions strongly influence SSA values of the biobased carbon materials. For instance, Akasaka et al. [5] prepared carbon materials from waste coffee beans under different activation methods and obtained carbon materials with SSA ranging from 780 to 1500 m^2 g^{-1}, where the highest SSA value was reached with KOH activation. Umpierres et al. [6] employed tucumã (Astrocaryum aculeatum) seed as a precursor to making carbon materials activated $ZnCl_2$. The authors reported that both chemicals simultaneously provide excellent textural with SSA reaching 1382 m^2 g^{-1}. Thue et al. [26] employed tucumã (*Astrocaryum aculeatum*) seed as a precursor to making carbon materials combining $ZnCl_2$/$NiCl_2$ as chemical activators. The authors reported that both chemicals simultaneously provide excellent textural with SSA reaching 1281 m^2 g^{-1}.

The differences in SSA values in Table 1 are related to the different activation mechanisms based on each chemical activator. For instance,

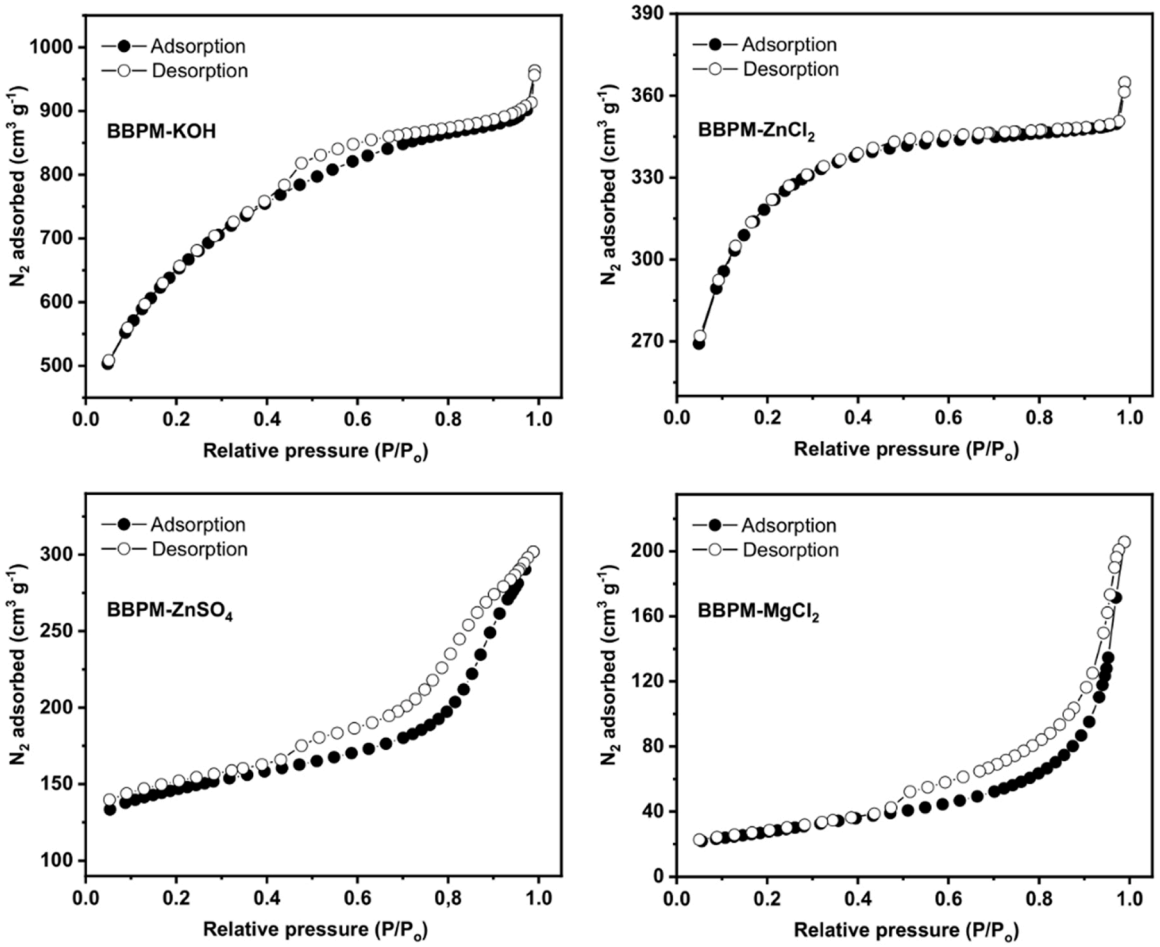

Fig. 1. Nitrogen adsorption-desorption isotherms for BBPM samples.

Table 1
Textural properties of the BBPM samples.

Samples	SSA (m^2 g^{-1})	A_{Micro} (m^2 g^{-1})	A_{Meso} (m^2 g^{-1})	Pore volume (cm^3 g^{-1})	Pore size (nm)
BBPM-KOH	2209	1710	499	1.49	2.70
BBPM-$ZnCl_2$	1018	562	456	0.56	2.22
BBPM-$ZnSO_4$	467	303	164	0.47	4.00
BBPM-$MgCl_2$	98	6	92	0.31	12.9

KOH activation consists of several steps during the pyrolysis process-based solid-liquid reactions because potassium hydroxide is diluted in water. Above 700 °C, potassium metallic is formed and may enhance the porosity; the metallic ion K^+ may act as a catalyst for gasification reactions, which helps to form and develop pore structures [31,32]. Also, a K intercalation process can occur; K ions may go between graphene layers of the BBPM, which widen the BBPM pore network and strain the structure. At high temperatures (e.g., 900 °C, the carbon network is so strained that it bursts, which potentializes the pore formation and reaches very high SSA values.

Activation with $ZnCl_2$, as a Lewis acid, is a potent dehydrating reagent as it catalyzes the decomposition of lignocellulosic compounds. This activation involves dehydration, depolymerization, and ring-opening [32–34]. $ZnCl_2$ is an efficient catalyst for C-O and C-C bonds scission. Moreover, during pyrolysis, $ZnCl_2$ starts to melt at 290 °C and may, if evenly mixed with the biomass, reach the biomass' interior. Increasing the pyrolysis temperature leads to thermal dehydration of the zinc oxide chloride hydrate that forms a gaseous phase of $ZnCl_2$ and a solid phase of zinc oxide. The gaseous phase of $ZnCl_2$ is diffused through the carbonaceous structure to develop the pore network [33,34].

Activation with $ZnSO_4$, zinc sulfate reacts with biomass during pyrolysis, inhibiting hemicellulose and promoting cellulose degradation [35]. Then, cellulose degradation becomes the primary reaction in the activation process. As zinc sulfate starts melting at 100 °C, it more easily reaches the cellulose and promotes the heating transfer, increasing cellulose degradation and further developing the porous materials' pore network. However, very few studies have dealt with $ZnSO_4$ and biomass activation; therefore, additional and deeper analysis needs to be carried out to understand the inner mechanism of how $ZnSO_4$ influences the pore formation during the biomass pyrolysis.

Activation with $MgCl_2$, like $ZnCl_2$, it is also a strong dehydrating reagent. First, when $MgCl_2$ powder and biomass are mixed with water, a hydrating product ($MgCl_2.6H_2O$) is formed [36–38]. Between 100 °C and 300 °C, it undergoes partial dehydration forming Mg(OH)Cl [36, 37]. Above 375 °C, formaldehyde and furfural are released, which means that depolymerization of cellulose occurs [36–38]. At temperatures higher than 600 °C, $MgCl_2$ decomposes directly to MgO to leave MgO particles within the pyrolyzed carbon matrix. MgO particles have an essential role in the activation process of biomass because magnesium oxide particles cannot be aggregated, and the final porous structure of is formed [37,38].

It is crucial to mention that the actual porosity, pore structures, and SSA are reached when the pyrolyzed samples are washed with HCl under reflux [39,40]. The HCl is responsible for extracting the inorganics from the pyrolyzed biomass structure, leaving voids, cavities, and pores to

form a well-developed porosity in the BBPM samples [39,40].

3.1.2. Scanning electron microscopy (SEM)

SEM analysis of BBPM helps illustrate the correlation between the chemical activation method and BBPM morphologies and the AMP adsorption performance. The SEM images (Fig. 2) confirm that the chemical activation agents provoke significantly different features of the BBPM surface; this strongly suggests that BBPMs can be easily modified by simply varying the type of chemical activator in combination with the pyrolysis process. The BBPM-KOH exhibits a sponge-like and extremely rough structure with many holes, cavities, and large macropores. This appearance suggests well-developed porosity and confirms the results of the textural and SSA analyses. The $ZnCl_2$-synthesized BBPM exhibits a broken and dense structure with holes and craters of different sizes and shapes, whereas preparation yields structures with smaller particles than the KOH- and $ZnCl_2$–activated samples - in addition, tiny holes are observed for the $ZnSO_4$-activated samples.

3.1.3. Raman spectroscopy (I_D/I_G)

Raman spectroscopy was carried out to analyze the degree of order/disorder and ratio of graphitization of the fabricated BBPM samples. The Raman spectra measured the I_D/I_G bands ratio [25,30] (see Supplementary Fig. S1). The lower I_D/I_G ratio implies that the carbon materials present orderly graphite structures with a high graphitization ratio. Conversely, a higher I_D/I_G ratio reveals the formation of amorphous carbon materials [25,30]. Supplementary Fig. S1 also showed that the chemical agent caused important differences in the carbon structures; $ZnSO_4$ and $MgCl_2$ exhibited the lowest (I_D/I_G) and therefore the highest graphitization degrees and more ordered structures, while $ZnCl_2$ and KOH had the highest values (highly disordered structures).

3.1.4. X-ray photoelectron spectroscopy (XPS)

The chemical states of the BBPM samples were analyzed using XPS. It was utilized to comprehend further the chemical treatments' effects on the biobased porous spruce bark materials composition.

Fig. 3 shows XPS spectra concerning C1s and O1s, respectively [25,38,41]. The sample activated with $ZnSO_4$ showed sulfur peaks. The deconvolution of the C1s spectrum shows that all BBPM samples present C═C (of graphitic/aromatic groups), C-C (hydrocarbon ~ 284.3 eV), ester or carboxylic acid O═C–O (~289.1 eV), carbonyl C-O (~287.5 eV), C-O in phenolic or alcohols or ether groups (~286.5 eV). It is essential to highlight that graphitic carbon is the primary constituent [25,41].

O1s spectra were deconvoluted to three oxygen chemical states with binding energies at around 530,8–531,2 eV, 532,6–533,1 eV, 534,8–536,3 eV. These binding energies could correspond to oxygen singly bonded to carbon in aromatic rings, in phenols and ethers (533.2–533.8 eV), or to oxygen double-bonded with carbon in carbonyl and quinone-like structures (530,8–531,2 eV) [25,41,42], confirming the presence of some functional groups on the ACs' surfaces.

O 1s deconvolution spectra show four prominent peaks (KOH has shown only three bands). The peaks at around 530 eV are assigned to the oxygen singly bonded to carbon in aromatic rings, in phenols and ethers present on BBPM surfaces, whereas at 531 eV can be related to the oxygen double bonded to carbon. The peak at around 532–533 eV is attributed to the oxygen linked to carbon by a single bond, and that at 535–537 eV are attributed to oxygen from adsorbed water molecules [25,41,42].

The high-resolution S 2p can be fitted to four peaks, where the two peaks located at 163.9 and 165.1 eV were assigned to C–S bonding, one located at 162.5 eV attributed to thiophene sulfur, and one located at 168.6 eV referred to oxidized sulfur [43]. The sulfur covalent bond in the carbon matrix can provide a more polarized carbon surface which could positively affect the adsorption properties by electrostatic attraction [43].

The quantitative data from XPS analysis is shown in Supplementary Table 2. A variation on the C content in the BBPM samples is observed, whereas KOH presented the lowest C content (86.6%), while the O content showed the largest content (10.5%). The highest O1s content on BBPM-KOH suggests that this carbon-based material presents a more oxygenated chemical function than the other carbon materials, especially for functional groups related to C-O-C, C-OH, and C═O. On the contrary, the other activator agents yielded carbon materials with very high carbon content and fewer oxygen functionalities on their surfaces.

3.1.5. Hydrophobic-hydrophilic balance (HI)

The surface characteristics of the BBPM samples were also analyzed by two solvent vapors adsorption with different polarities, water (polar) and n-heptane (non-polar) [8,25,30,44]. The hydrophobic-hydrophilic ratio (HI) of a material suggests its tendency in adsorbing compounds that are organic or water-based [8,25,30,44]. The ratio of n-heptane to water uptake, in mass, for the four BBPM samples are presented as follows 1.19, 1.11, and 1.23 and 3.46 for KOH, $ZnCl_2$, $ZnSO_4$and $MgCl_2$, respectively. The first three have shown similar values, whereas the porous material activated with $MgCl_2$ has a much higher HI (3.46). Thus, the $MgCl_2$ has a more hydrophobic surface, which affects the AMP adsorption process.

The hydrophobic/hydrophilic behavior depends on the number of functional groups present on the AC's surface, the AC's aromatization rate, and the chemical nature of the biomass precursor [14,25,35].

3.1.6. Water vapor adsorption

The water vapor adsorption isotherms for the BBPM samples show that the chemical agents yielded dissimilar water vapor adsorption-desorption curves (see supplementary Fig. 3). KOH, $ZnCl_2$, and $ZnSO_4$-activated BBPMs present curves close to type IV, while the BBPM- $MgCl_2$ is closer to type I. Type IV isotherm describes the adsorption by a swellable hydrophilic solid until maximum hydration of sites is reached [45]. For type I, a high vapor uptake occurs under low relative humidity [45]. Although the isotherms of KOH, $ZnCl_2$, and $ZnSO_4$ samples are similar, the hysteresis's shape, form, and size are slightly different, indicating that the chemical activators influence the BBPM characteristics in different ways.

The water vapor adsorption is not solely influenced by the textural properties of the carbon materials; instead, its chemical properties are of higher importance [26]. However, high SSA and pore size distribution can optimize the water adsorption because a higher SSA can maximize the contact between the water and the carbon material; also, bigger pores in the range of mesoporosity are wide enough to facilitate the penetration of the water molecules in the interior of the solid and therefore increase the adsorbed volume. In this sense, the samples with the highest SSA also presented the highest water uptake. However, KOH and $ZnCl_2$ displayed almost the exact change in mass (adsorbed water amount), but BBPM-KOH exhibited a much high SSA; this suggests that water vapor sorption does not depend on one specific material property but several factors such as surface chemistry, hydrophilicity, SSA, and pore size distribution [26,30] (Fig. 4).

3.2. Adsorption study

3.2.1. Effect of pH of acetaminophen solution on its adsorption process

The initial pH of the adsorbate solution is a critical factor in the adsorption process since it influences both the existing adsorbate solution speciation and the adsorbent's surface charge [46].

Fig. 5 shows the q vs. the initial pH of acetaminophen solution. For pH values 3–9, the q values were practically constant. These outcomes suggest that the primary adsorption mechanism acting for acetaminophen onto BBPM samples could not be an electrostatic mechanism because it is independent of pH value [5,7,8,46]. Instead, pore-filling should be the most dominant mechanism of adsorption, which will be discussed later.

The literature corroborates these results: Nguyen et al. [46]

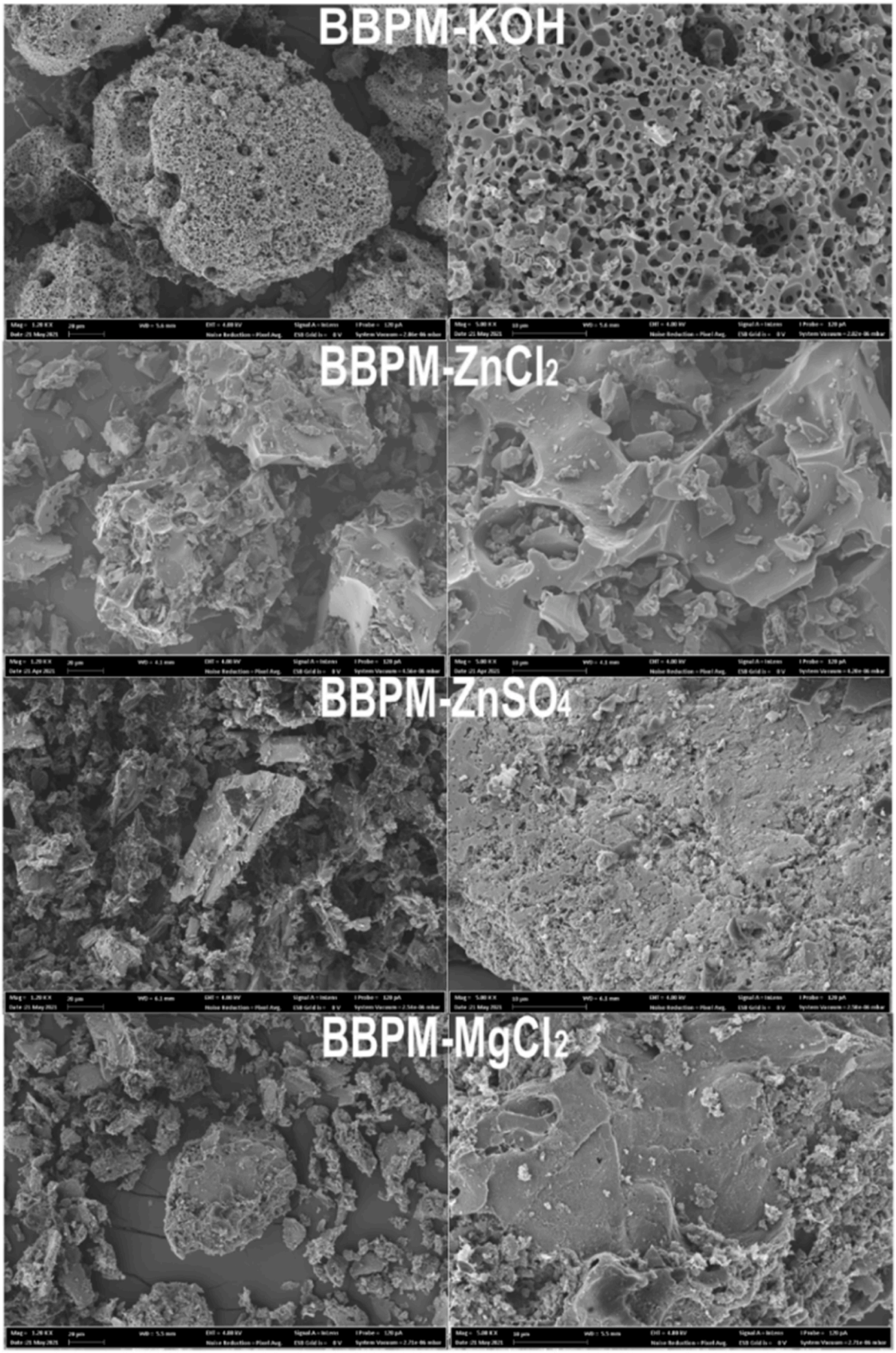

Fig. 2. SEM micrographs of BBPM samples.

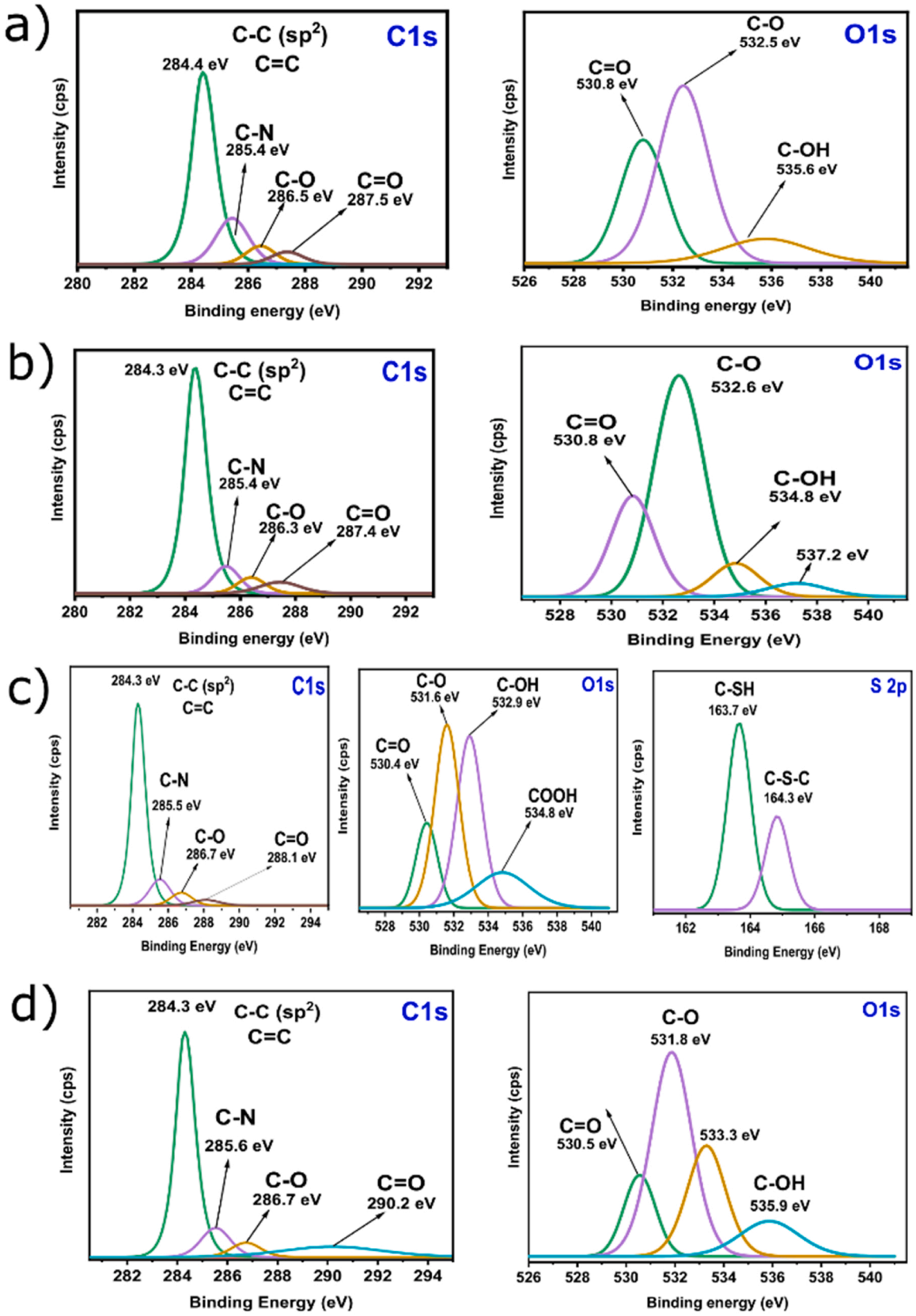

Fig. 3. XPS analysis for BBPM-KOH (a), BBPM-$ZnCl_2$ (b), BBPM-$ZnSO_4$ (c), and BBPM-$MgCl_2$ (d).

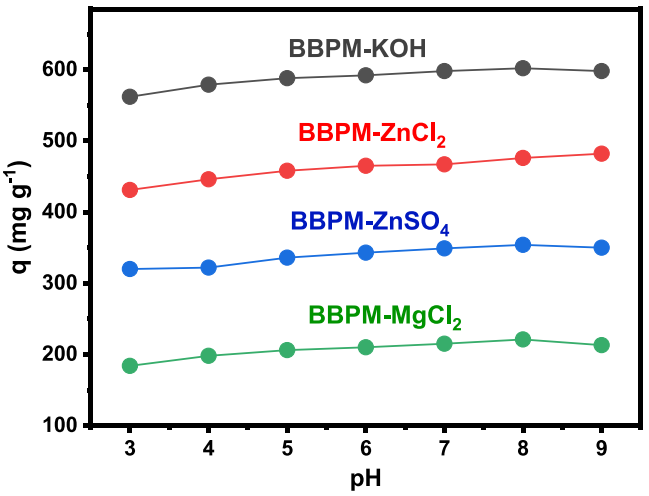

Fig. 4. Effect of initial pH on the acetaminophen sorption capacity. Adsorption experimental conditions: the initial adsorbate concentration was 1000 m L^{-1}, contact time of 120 min; a temperature of 23 °C; adsorbent dosage of 1.5 g L^{-1}, initial pH adsorbate solution 3.0–9.0.

employed commercial AC in the acetaminophen adsorption. The pH was varied from 2 to 10 and found that the adsorption capacity was kept practically constant within this pH interval. Therefore, no pH influence was reported. Saucier et al. [47] reported the same results and conclusions.

Based on the pH studies, further adsorption experiments were carried out with acetaminophen solutions with pH 6.0 (pH of the used deionized water); therefore, it was unnecessary to make any pH adjustments when the solution pH is within 3.0–9.0. The same goes for synthetic effluents.

3.2.2. *Kinetic of adsorption*

The kinetic process was evaluated in this work by applying three adsorption kinetic models (pseudo-first-order, pseudo-second-order, General order) to describe the intrinsic adsorptive constants mathematically. The contact time was evaluated up to 180 min at an initial 500 mg L^{-1} of AMP. Fig. 5 shows kinetic curves for the four BBPM. It shows that the adsorption process occurred extremely fast, with the equilibrium being reached at the very first minutes for all four samples (see Fig. 5). The highly rapid adsorption at the first minutes of the kinetic is due to the abundant available active sites that easily adsorb AMP molecules on either surface and pore structures of the BBPM samples. These results suggest that all BBPM samples had a very high affinity to AMP.

Also, at 500 mg L^{-1} AMP, a high abundance of active sites exist that need to be fulfilled; this leads to a high driving force for the mass transfer from the bulk solution to the BBPM surfaces, resulting in extremely fast adsorption [46,47]. What could explain the fastness in the adsorption rate of AMP on BBPM samples and the vast presence of sites of adsorptions are the porosity, presence of functional groups on the BBPM surfaces, and hydrophobicity-hydrophilicity data of the BBPM samples; AMP molecule has a maximum diagonal length of 0.88 nm [46,47], and all BBPM samples have well-developed micro and mesoporosity, and with high pore volumes [46,47], this makes more accessible to the AMP molecule be accommodated into the pores of the BBPM samples.

In addition, AMP has a dipole moment of 3.63 Debye, HLB

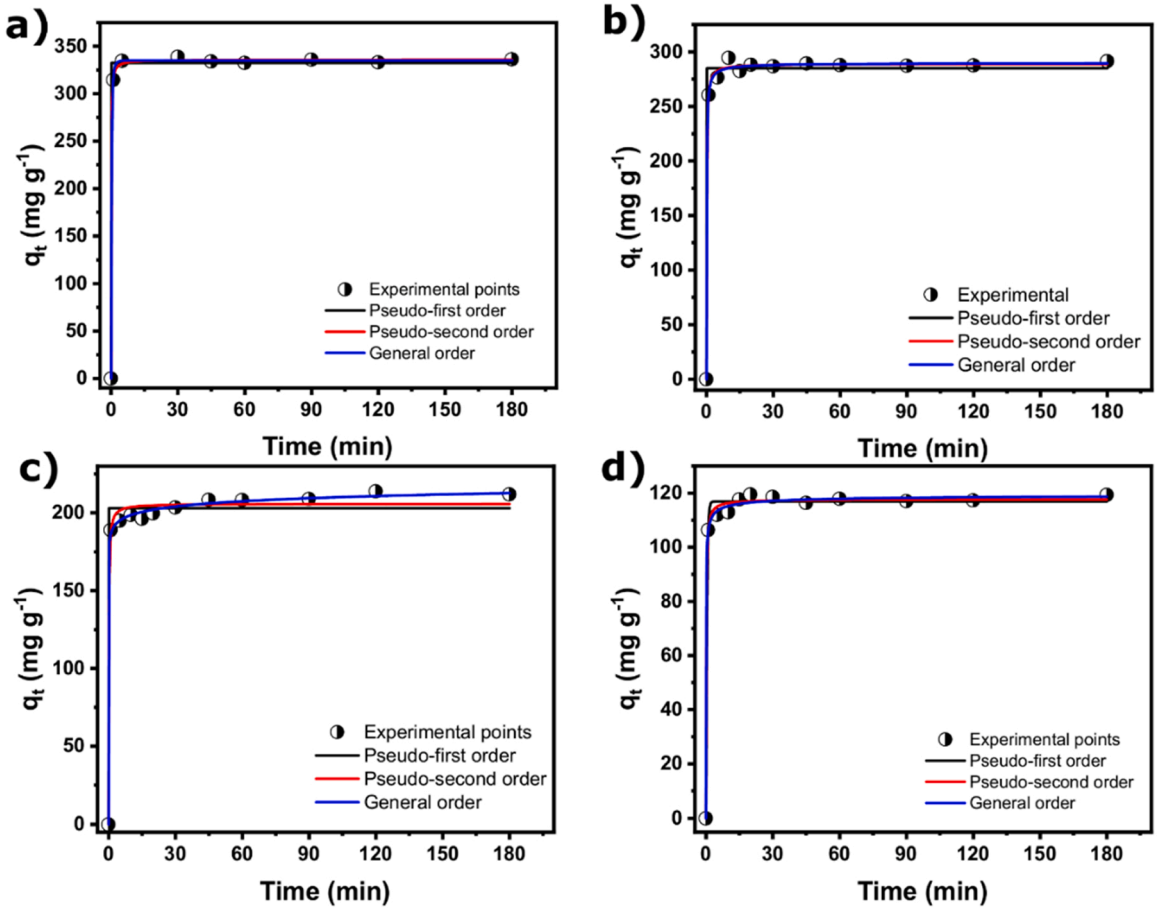

Fig. 5. Acetaminophen kinetics of adsorption curves onto BBPM-KOH (a) BBPM-$ZnCl_2$ (b) BBPM-$ZnSO_4$ (c) BBPM-$MgCl_2$ (D). Condition: Initial pH of 6.0, 1.5 g L^{-1} adsorbent dosage, 23 °C.

(Hydrophilic-lipophilic balance) of 6.53–9.53, showing that AMP has a predominantly hydrophilic behavior [46,47] with an intermediate affinity to water and has some affinity to polar groups such as -OH, C═O, O-C═O, and -NH present on BBPM surfaces. The hydrophilic groups present on BBPM surfaces improve the wettability of the BBPM structure and the access of the acetaminophen to the active sites of the BBPMs. Also, it is essential to highlight that the pores and interconnect porous structures of the carbon-based materials present active sites, allowing a fast and efficient adsorption process.

Table 2 shows the parameters of the kinetic models used to fit the experimental data. The models' fitness was evaluated according to the adjusted determination coefficient (R^2_{adj}), and standard deviation of residues (SD). Lower SD and higher R^2_{adj} values indicate a smaller difference between experimental and theoretical q values (given by the models) and therefore have the best suitable model. Based on these parameters, the General order model had the highest R^2_{adj} and lowest SD values for all four carbons (see Table 2).

The general order kinetics describes that the order of the adsorption process should be the same as that of a chemical reaction [6,26]. In a chemical reaction, the reaction order is measured experimentally [6,26]. The general order kinetic equation presents different values for n (order of adsorption rate) when the concentration of the adsorbate is changed, making it difficult to compare the kinetic parameters of the model [6,26]. So, $t_{0.5}$ and $t_{0.95}$ were used to compare the kinetics of adsorption of acetaminophen on biochars [6,26]. $t_{0.5}$ is the time to obtain half of saturation (qe) in the kinetic results, $t_{0.95}$ was the time to obtain 95% of the saturation (qe). $t_{0.5}$ and $t_{0.95}$ were calculated and shown based on the best fitted model (General order).

The characteristic adsorption of the AMP on all BBPM samples presented similar behaviors but with differences in the times. For BBPM samples, the calculated $t_{0.5}$ and $t_{0.95}$ from the general order kinetic model showed that 50% and 95% of equilibrium sorption capacity were obtained at 0.1750 and 1.111 min (BBPM-KOH), 0.08747 and 2.408 min (BBPM-$ZnCl_2$), 0.1060 and 1.992 (BBPM-$ZnSO_4$), and 0.03431 and 4.086 (BBPM-$MgCl_2$). Rapid adsorption of the AMP on all four BBPM indicated a high affinity between the adsorbate molecules and the BBPM surface.

Adsorption of AMP by the BBPM samples is a multi-step process. This process involves transporting AMP molecules from the solution phase to the BBPM's surfaces and then AMP diffusion into BBPM's pores. Since BBPM samples are porous materials, the intraparticle diffusion curves further explored the fast and efficient AMP adsorption. Supplementary Fig. 4 shows the plots of qt versus $\sqrt{t}$ for all four BBPM samples. The BBPM-KOH and BBPM-$MgCl_2$ presented only one stage of the rate of adsorption. Therefore, this stage can be assigned as the combination of the diffusion of the AMP molecules to the BBPM surfaces and the intraparticle diffusion, which both were extremely fast, reaching the equilibrium at the very first minutes. On the other hand, BBPM-$ZnCl_2$ and BBPM-$ZnSO_4$ presented two stages, where the first can be related to boundary diffusion and intraparticle diffusion into the adsorbent pores, which is faster in the BBPM- $ZnCl_2$ sample, which may be due to the higher number of mesopores that could offer less resistance to liquid penetration when compared to the micropores. In the second stage, the acetaminophen was adsorbed and diffused into the interior site of the BBPM samples until attaining equilibrium.

3.2.3. Equilibrium of adsorption

The presentation of adsorption isotherm has enormous significance in understanding and designing an efficient adsorption process. Therefore, among several models, Langmuir, Freundlich, and Liu isotherms were chosen to evaluate the AMP fitness onto BBPM samples.

As for the kinetic studies, R^2_{adj} and SD values were used to evaluate the suitability of the isotherm models. Therefore, Liu was found to be the best model for AMP adsorption on BBPM samples. It was, therefore, used to describe the relationship between AMP and the PPBM adsorption system. This isotherm model can be applied to both homogenous and heterogeneous systems, and it has a hybrid adsorption mechanism, which does not follow ideal monolayer adsorption. This is highlighted because Freundlich did not provide a good fit for the experimental adsorption data (see supplementary Fig. 5 and Table 3). This suggests that the adsorption process of acetaminophen on the three biochars was more homogenous than heterogeneous.

The maximum adsorption capacities (Q_{max}) were 752.7, 429.6, 364.8 and 321.2 mg g^{-1} for BBPM-KOH, BBPM-$ZnCl_2$, BBPM-$ZnSO_4$, and BBPM-$MgCl_2$, respectively. Obviously, the porous material treated with KOH presented the best performance compared to the others; it seems that the SSA played a huge influence on the AMP adsorption process since the samples with the highest SSA values also had the highest sorption capacities. However, if it is paid attention in detail, the SSA was not the only factor that influenced the Q_{max} because BBPM-KOH has an

Table 2
Kinetic parameters of acetaminophen adsorption onto BBPM samples.

Model	Acetaminophen initial concentration (500 mg L^{-1})			
	BBPM-KOH	BBPM-$ZnCl_2$	BBPM-$ZnSO_4$	BBPM-$MgCl_2$
Pseudo-first order				
q_1 (mg g^{-1})	332.5	284.9	203.1	116.9
k_1 (min^{-1})	62.51	53.64	38.82	2.400
R^2	0.9960	0.9885	0.9837	0.9954
R^2_{adj}	0.9954	0.9873	0.9820	0.9949
SD (mg g^{-1})	7.515	9.312	7.922	2.406
Pseudo-second order				
q_2 (mg g^{-1})	334.1	289.0	205.9	117.6
k_2 (g mg^{-1} min^{-1})	0.04539	0.03077	0.04578	0.0741
R^2	0.9996	0.9981	0.9920	0.9972
R^2_{adj}	0.9995	0.9969	0.9913	0.9969
SD (mg g^{-1})	2.481	3.826	5.531	1.877
General order				
q_n (mg g^{-1})	335.1	289.9	412.8	119.9
k_n (min^{-1} (g $mg^{-1})^{n-1}$)	0.7467	0.01216	0.002654	0.001850
n	1.305	2.222	43.51	3.108
$t_{0.5}$	0.1750	0.08747	0.1060	0.03431
$t_{0.95}$	1.111	2.408	1.992	4.086
R^2	0.9997	0.9981	0.9988	0.9979
R^2_{adj}	0.9996	0.9977	0.9985	0.9975
SD (mg g^{-1})	2.206	3.817	5.012	1.696

Table 3
Equilibrium parameters of acetaminophen adsorption onto BBPM samples.

Model	Bio-based carbon materials samples			
	BBPM-KOH	BBPM-$ZnCl_2$	BBPM-$ZnSO_4$	BBPM-$MgCl_2$
Langmuir				
q_e (mg g^{-1})	571.0	411.1	363.0	222.5
k_1 (min^{-1})	0.6483	0.1933	0.02142	0.03435
R^2	0.9532	0.9904	0.9570	0.9383
R^2_{adj}	0.9474	0.9893	0.9522	0.9322
SD (mg g^{-1})	49.85	15.81	29.46	21.22
Freundlich				
k_F ((mg g^{-1})(mg $L^{-1})^{-1/nF}$)	248.3	143.3	41.55	51.47
n_F (dimensionless)	5.774	5.161	2.847	4.460
R^2		0.9322	0.9811	0.9741
R^2_{adj}	0.9739	0.9247	0.9791	0.9715
SD (mg g^{-1})	37.27	41.96	19.50	13.76
Liu				
Q_{max} (mg g^{-1})	752.7	429.6	364.8	321.2
Kg (L mg^{-1})	0.1523	0.1651	0.1330	0.08610
n_L (dimensionless)	0.4128	0.7922	0.4759	0.4343
R^2	0.9903	0.9949	0.9840	0.9863
R^2_{adj}	0.9880	0.9936	0.9800	0.9832
SD (mg g^{-1})	23.83	12.17	19.00	10.54

SSA of 2209 m^2 g^{-1} while BBPM-$MgCl_2$ has only 98 m^2 g^{-1}, an SSA roughly 22 times higher; however, Q_{max} for BBPM-KOH is only 2.3 times higher compared to the Q_{max} of BBPM-$MgCl_2$, this strongly suggests that the surface chemistry also played a huge role on the AMP adsorption onto BBPM-$MgCl_2$. The same for BBPM-$ZnSO_4$ presented an SSA of 467 m^2 g^{-1} and a Q_{max} of 344 mg g^{-1}, almost the same as BBPM-ZnCl2, which has more than one double of SSA value (1018 m^2 g^{-1}).

The FTIR and XPS results support the information that BBPM-$ZnSO_4$ and BBPM-$MgCl_2$ showed more functionalities on their surfaces. In addition, something that should be pointed out is that BBPM-$MgCl_2$ showed to be much more hydrophobic than others (see Fig. X); this could also have influenced the AMP adsorption performance.

3.2.4. Acetaminophen adsorption: comparison with literature

In this work, previous acetaminophen adsorption studies strongly indicated that the spruce bark carbon materials presented efficient removals from aqueous solutions. Although the nature of every carbon material is different, and each one has its own merits and demerits, supplementary Table 2 provides a comparison data between our carbons with others found in the literature [7,46–52]. It is essential to point out that in each work presented in the supplementary Table 2, its Q_{max} values were acquired through the best-optimized experimental conditions.

As can be seen, among all sorbents, the BBPM-KOH presented the highest adsorption capacity, followed by BBPM- $ZnCl_2$ that presented the second highest values among all adsorbents, showing competitiveness in removing emerging pollutants from waters and possibly many other organic and inorganic compounds from wastewaters. It is well known that SSA strongly influences the adsorption of emerging pollutants. However, the carbon material with the highest SSA did not present the highest Q_{max}. On the other hand, BBPM-KOH displayed the second-highest SSA and the highest Q_{max} for acetaminophen values.

Interestingly, (BBPM- $MgCl_2$) [resented the second-lowest SSA values among the sorbents presented in supplementary Table 2 (98 m^2 g^{-1}) but yet so, presented one the highest Q_{max}. This highlights that although SSA is a crucial parameter in the adsorption process, it is not the only one that influences the process, but also the surface groups, pore size, volume, etc.

3.2.5. Acetaminophen mechanism of adsorption

Based on the physicochemical properties of the BBPM materials such as SSA and porosity, pore size distribution, HI results, surface functionalities, and adsorption data (initial pH solution, the kinetics of adsorption, and equilibrium studies), it is possible to state the possible mechanisms that are acting in the AMP adsorption onto BBPM adsorbents (see Fig. 6).

Based on the pH study results, the electrostatic attraction was not the major contributor to the AMP removal since it depends on the pH. However, since the BBPM materials showed to be hydrophobic and to have many functional groups on their surfaces, some interactions such as hydrogen bonds, π–π interactions, hydrophobic interactions (van der Walls), of the functional groups of the acetaminophen with the groups of the BBPM occur [46,47].

Considering the above considerations, the pore-filling process due to the well-developed pore structure and elevated SSA values contributed more to the AMP adsorption onto the BBPM. In addition, the pore-filling mechanism was maximized due to the dimensions of the acetaminophen molecule (1.19 nm (length), 0.75 nm (width), and 0.46 nm (thickness)); it is expectable it can easily access the wider and some of the narrower micropores as well as mesopores.

3.2.6. Regeneration studies

The BBPM samples were also subjected to regeneration studies. The samples were subjected to four adsorption-desorption cycles. All four BBPM samples were saturated with 100% of their capacity with an adsorbent dosage of 1.5 g L^{-1}, and two eluents were employed in the adsorption cycles (solutions of 0.1 M NaOH + 20% EtOH and 0.25 M NaOH + 20% EtOH) [7,47].

Fig. 7 shows that the eluent 0.1 M NaOH + 20% EtOH resulted in a better cyclability efficiency. On the other hand, the lower efficiency for the 0.25 M NaOH + 20% EtOH eluent could be explained because the higher concentration of NaOH could compete with the acetaminophen molecules, which can cover the BBPM surfaces and get trapped into their small pores.

With the eluent 0.1 M NaOH + 20% EtOH, the 2nd cycle adsorbed roughly 80% of the acetaminophen, the 3rd cycle removal was approximately 70%, while in the 3rd cycle, the removal was below 50% for all four samples. This decrease can be caused by acetaminophen molecules seized in the smaller pores of the BBPM, which then are difficult to remove by the eluent [7,47].

Based on the above results, the BBPM exhibited good reusability even after 3rd cycle. However, further experiments and testing of different eluents could help the BBPM reach even higher adsorption performances after three or more cycles.

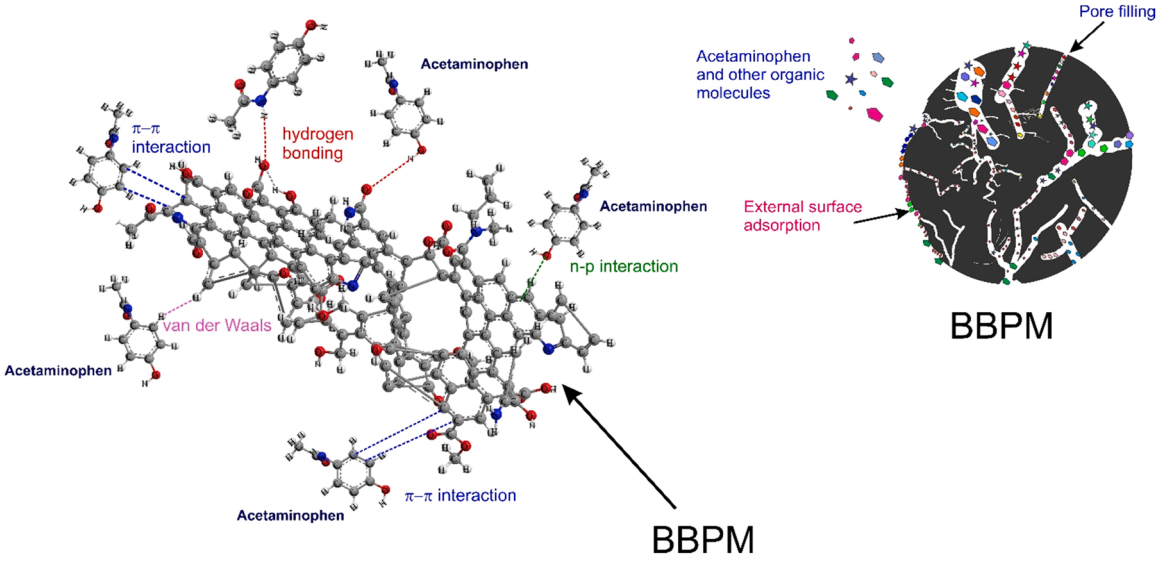

Fig. 6. Mechanism of adsorption for acetaminophen on BBPM structure.

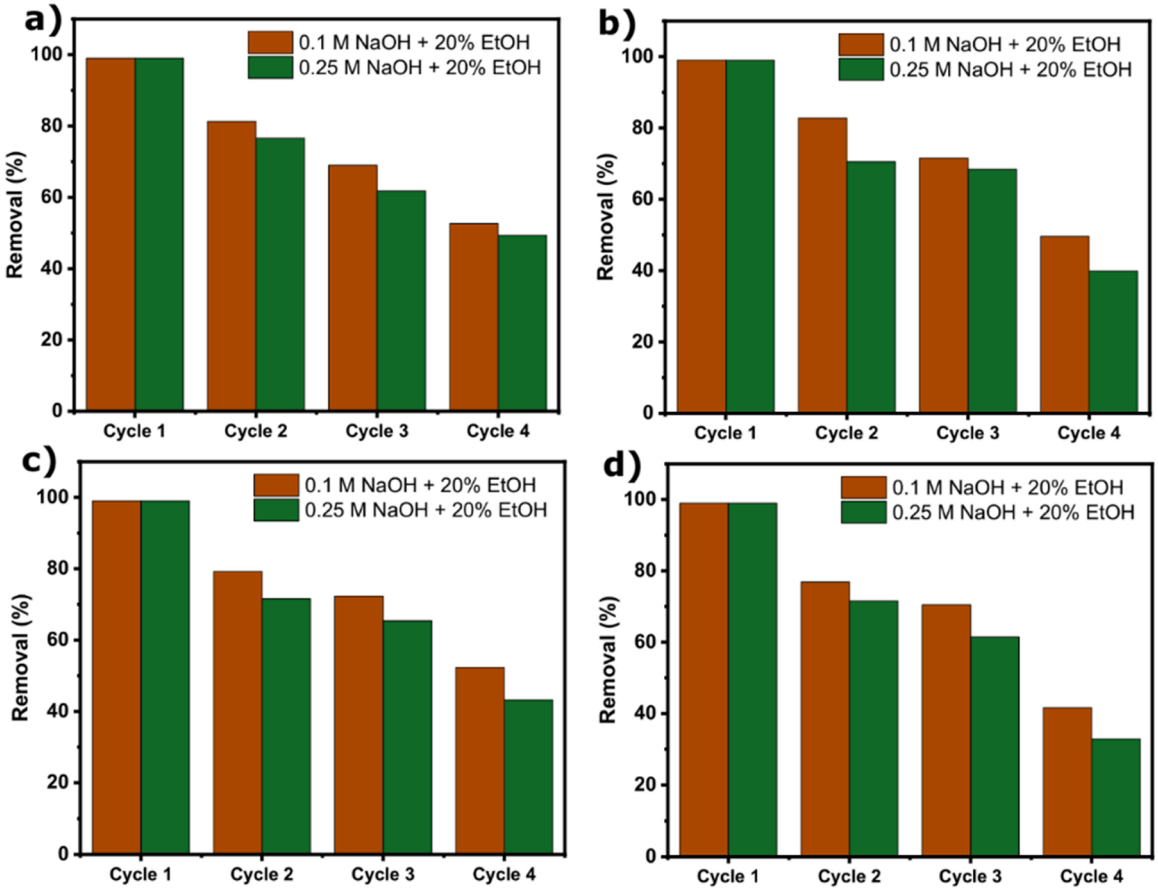

Fig. 7. Cycles of adsorption of acetaminophen on BBPM-KOH (a), BBPM-$ZnCl_2$ (b), BBPM-$ZnSO_4$ (c) and BBPM-$MgCl_2$ (d).

3.2.7. Synthetic wastewater treatment tests

Since the BBPM materials were successfully employed in the acetaminophen removal, we also employed them to remove synthetic effluents. Therefore, it was expected that the BBPM samples could be effectively applied in treating wastewaters composed of similar compounds found in effluents of drugs industries. For that, two synthetic effluents composed of seven drugs and other organic and inorganic compounds (see supplementary Table 1) were employed to test the efficiency of the BBPM samples to clean them up (see Fig. 8).

The calculation of the percentage removal was done taking into account the areas under the UV–vis spectra from 190 to 400 nm of the two synthetic effluents before and after the treatment [7] (see Fig. 8).

The spectra curves show that all BBPM samples exhibited interesting percentage removals for both effluents: the percentage removal of effluent A were 91.9%, 87.3%, 81.5%, and 49.1% for KOH-BBPM, $ZnCl_2$-BBPM, $ZnSO_4$-BBPM and $MgCl_2$-BBPM, respectively; while for the effluent B were 90.3%, 79.9%, 76.3%, and 40.2% for KOH-BBPM, $ZnCl_2$-BBPM, $ZnSO_4$-BBPM and $MgCl_2$-BBPM, respectively. The percentage order followed the same as the acetaminophen adsorption and S_{BET} area values. Thus, the above results strongly support the practical application of the biochars in treating real pharmaceutical wastewaters.

4. Conclusion

In summary, our study developed new porous carbon materials for efficient emerging pollutants removal through a facile and one-step activation method. Furthermore, using sustainable, low cost and abundant biomass precursor (Norway spruce bark) to develop these novel porous carbon materials promoted the tenets of green chemistry. The characterization data proved that the different chemical agents primarily affected the physicochemical properties. The evident influence of the chemical activators was observed on SSA values, KOH (2209 $m^2 g^{-1}$), $ZnCl_2$ (1019 $m^2 g^{-1}$), $ZnSO_4$ (446 $m^2 g^{-1}$), and $MgCl_2$ (98 $m^2 g^{-1}$). The activation of $MgCl_2$ yielded three times more hydrophobic material than the other activation methods. The carbon materials were successfully employed to adsorb acetaminophen, and the samples with the highest SSA exhibited the best adsorption performances. The kinetics data indicated ultrafast acetaminophen adsorption equilibriums, equal to 1 min for KOH and $MgCl_2$ and 15 min for $ZnSO_4$ and $ZnCl_2$. The adsorption mechanism suggests that the pore-filling mechanism mainly dominates the acetaminophen removal, although electrostatic attraction forces are also involved in the process. The BBPM regeneration studies showed good cyclability at around 70% in the 3rd cycle. The samples were also used to treat two synthetic effluents, which attained a removal percentage up to 91.9%. The results from this study strongly suggest that Norway spruce bark is a promising precursor for bio-based carbon materials with high efficiency in removing emerging pollutants from effluents.

Future works

(i) To study the effect of pyrolysis parameters (temperature and holding time) and the effect of chemical activator amount (ratio between biomass precursor and chemical activator) on BBPM properties because synergetic effects between these parameters can play a significant role on the physicochemical properties of the carbon materials as well as on their adsorption performance, the generation of synergistic effects and the understanding of their functional mechanisms need to be further examined.

(ii) The other selection of suitable biomass sources and the development/optimization of corresponding cost-effective synthesis

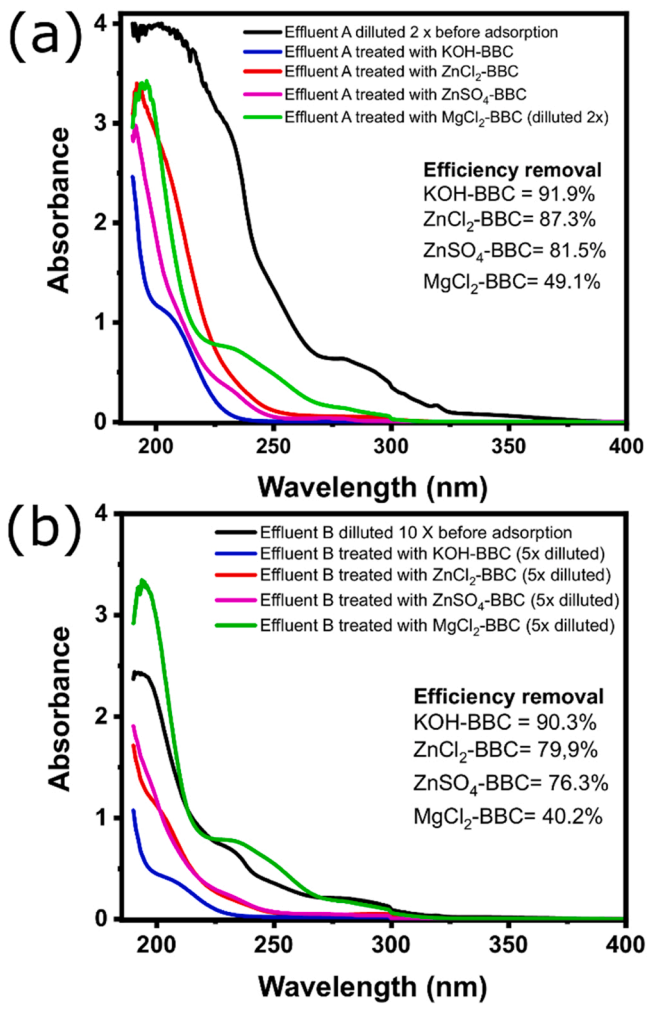

Fig. 8. Effluents spectra of non-treated and treated with BBPM materials.

methods to achieve high-performance biomass-derived carbon materials and their chemical activators.

(iii) The exploration of possible opportunities for not only spruce bark carbon materials but any kind of biomass-derived carbon materials to obtain sustainable, versatile, and efficient carbon materials for environmental and a wide range of other applications.

CRediT authorship contribution statement

Glaydson Simoes dos Reis: Conceptualization, Software, Data curation, Investigation, Methodology, Writing – original draft, Writing – review & editing. **Marine Guy**: Investigation, Methodology. **Manon Mathieu:** Investigation, Methodology. **Mohamed Jebrane**: Writing – review & editing. **Eder Claudio Lima**: Software, Data curation, Writing – review & editing. **Mikael Thyrel**: Writing – review & editing. **Guilherme Dotto**: Writing – review & editing. **Sylvia H. Larsson**: Writing – review & editing, Funding acquisition,

Declaration of Competing Interest

The authors declare that they have no known competing financial interests or personal relationships that could have appeared to influence the work reported in this paper.

Acknowledgments

This research was funded by the Treesearch Postdoctoral program and Bio4Energy— a Strategic Research Environment appointed by the Swedish government, and the Swedish University of Agricultural Sciences. Guy and Mathieu thank ERASMUS for the financial support. The FTIR and Raman measurements were performed at the Vibrational Spectroscopy Core Facility (ViSp), Chemical Biological Centre (KBC), Umeå University. The Umeå Core Facility for Electron Microscopy (UCEM-NMI node) at the Chemical Biological Centre (KBC), Umeå University, is gratefully acknowledged.

Appendix A. Supporting information

Supplementary data associated with this article can be found in the online version at doi:10.1016/j.colsurfa.2022.128626.

References

[1] H. Marsh, F. Rodríguez-Reinoso, Activated Carbon, Elsevier Science, 2006.
[2] G.S. dos Reis, S.H. Larsson, H.P. Oliveira, M. Thyrel, E.C. Lima, Sustainable biomass activated carbons as electrodes for battery and supercapacitors—a mini-review, Nanomaterials 10 (2020) 1398.
[3] J. Wang, H. Kong, J. Zhang, Y. Hao, Z. Shao, F. Ciucci, Carbon-based electrocatalysts for sustainable energy applications, Prog. Mater. Sci. 116 (2021), 100717.
[4] T. Kopac, Hydrogen storage characteristics of bio-based porous carbons of different origin: a comparative review, Int. J. Energy Res. 45 (2021) 20497–20523.
[5] H. Akasaka, T. Takahata, I. Toda, H. Ono, S. Ohshio, S. Himeno, T. Kokubu, H. Saitoh, Hydrogen storage ability of porous carbon material fabricated from coffee bean wastes, Int. J. Hydrog. Energy 36 (2011) 580–585.
[6] C.S. Umpierres, P.S. Thue, G.S. dos Reis, I.A.S. de Brum, E.C. Lima, W.A. de Alencar, S.L.P. Dias, G.L. Dotto, Microwave activated carbons from Tucumã (*Astrocaryum aculeatum*) waste for efficient removal of 2-nitrophenol from aqueous solutions, Environ. Technol. 39 (2018) 1173–1187.
[7] D.R. Lima, A. Hosseini-Bandegharaei, P.S. Thue, E.C. Lima, Y.R.T. de Albuquerque, G.S. dos Reis, C.S. Umpierres, S.L.P. Dias, H.N. Tran, Efficient acetaminophen removal from water and hospital effluents treatment by activated carbons derived from Brazil nutshells, Colloid Surf. A 583 (2019), 123966.
[8] F.M. Kasperiski, E.C. Lima, C.S. Umpierres, G.S. dos Reis, P.S. Thue, D.R. Lima, S.L. P. Dias, C. Saucier, J.B. da Costa, Production of porous activated carbons from *Caesalpinia ferrea* seed pod wastes: Highly efficient removal of captopril from aqueous solutions, J. Clean. Prod. 197 (2018) 919–929.
[9] L. Leng, Q. Xiong, L. Yang, H. Li, Y. Zhou, W. Zhang, S. Jiang, H. Li, H. Huang, An overview on engineering the surface area and porosity of biochar, Sci. Total Environ. 763 (2021), 144204.
[10] V. Piergrossi, C. Fasolato, F. Capitani, G. Monteleone, P. Postorino, P. Gislon, Application of Raman spectroscopy in chemical investigation of impregnated activated carbon spent in hydrogen sulfide removal process, Int. J. Environ. Sci. Technol. 16 (2019) 1227–1238.
[11] D. Bergna, T. Varila, H. Romar, U. Lassi, Comparison of the Properties of Activated Carbons Produced in One-Stage and Two-Stage Processes, 2018, p. 41. C 4.
[12] M. Kılıc, E. Apaydın-Varol, A.E. Pütün, Preparation and surface characterization of activated carbons from *Euphorbia rigida* by chemical activation with $ZnCl_2$, K_2CO_3, NaOH, and H_3PO_4, Appl. Surf. Sci. 261 (2012) 247–254.
[13] Z. Yuan, Z. Xu, D. Zhang, W. Chen, T. Zhang, Y. Huang, L. Gu, H. Deng, D. Tian, Box-Behnken design approach towards optimization of activated carbon synthesized by co-pyrolysis of waste polyester textiles and $MgCl_2$, Appl. Surf. Sci. 427 (2018) 340–348.
[14] T. Kopac, F.O. Erdogan, Temperature and alkaline hydroxide treatment effects on hydrogen sorption characteristics of multi-walled carbon nanotube–graphite mixture, J. Indus. Eng. Chem. 15 (2009) 730–735.
[15] S. Jansen, H. Konrad, T. Geburek, The extent of historic translocation of Norway spruce forest reproductive material in Europe, Ann. For. Sci. 74 (2017) 56.
[16] J. Krogell, B. Holmbom, A. Pranovich, J. Hemming, S. Willför, Extraction and chemical characterization of Norway spruce inner and outer bark, Nord. Pulp Pap. Res. J. 27 (2012) 6–17.
[17] J.G. Bessems, N.P. Vermeulen, Paracetamol (acetaminophen)-induced toxicity: molecular and biochemical mechanisms, analogues and protective approaches, Crit. Rev. Toxicol. 31 (2001) 55–138.
[18] C. Sophia, E.C. Lima, Removal of emerging contaminants from the environment by adsorption, Ecotoxicol. Environ. Saf. 150 (2018) 1–17.
[19] J. Żur, A. Piński, A. Marchlewicz, K. Hupert-Kocurek, D. Wojcieszyńska, U. Guzik, Organic micropollutants paracetamol and ibuprofen—toxicity, biodegradation, and genetic background of their utilization by bacteria, Environ. Sci. Pollut. Res. 25 (2018) 21498–21524.
[20] S. Ottoboni, M. Simurda, S. Wilson, A. Irvine, F. Ramsay, C.J. Price, Understanding effect of filtration and washing on the dried product: paracetamol case study, Powder Technol. 366 (2020) 305–323.
[21] W.C. Yun, K.Y.A. Lin, W.C. Tong, Y.F. Lin, Y. Du, Enhanced degradation of paracetamol in water using sulfate radical-based advanced oxidation processes catalyzed by 3-dimensional Co3O4 nanoflower, Chem. Eng. J. 373 (2019) 1329–1337.

[22] C. Postigo, S.D. Richardson, Transformation of pharmaceuticals during oxidation/disinfection processes in drinking water treatment, J. Hazard. Mater. 279 (2014) 461–475.
[23] E. Moctezuma, E. Leyva, C.A. Aguilar, R.A. Luna, C. Montalvo, Photocatalytic degradation of paracetamol: Intermediates and total reaction mechanism, J. Hazard. Mater. 243 (2012) 130–138.
[24] A.B. Leite, C. Saucier, E.C. Lima, G.S. dos Reis, C.S. Umpierres, B.L. Mello, M. Shirmardi, S.L.P. Dias, C.H. Sampaio, Activated carbons from avocado seed: optimization and application for removal several emerging organic compounds, Environ. Sci. Pollut. Res. 25 (2018) 7647–7661.
[25] G.S. dos Reis, S.H. Larsson, M. Thyrel, M. Mathieu, P.N. Tung, Application of design of experiments (DoE) for optimised production of micro-and mesoporous Norway spruce bark activated carbons, Biomass Conv. Bioref. (2021), https://doi.org/10.1007/s13399-021-01917-9.
[26] E.C. Lima, M.H. Dehghani, A. Guleria, F. Sher, R.R. Karri, G.L. Dotto, H.N. Tran, CHAPTER 3 - Adsorption: Fundamental aspects and applications of adsorption for effluent treatment, in: M. Hadi Dehghani, R. Karri, E. Lima (Eds.), Green Technologies for the Defluoridation of Water, Elsevier, 2021, pp. 41–88.
[27] Y.L. de, O. Salomón, J. Georgin, G.S. dos Reis, É.C. Lima, M.L.S. Oliveira, D.S. P. Franco, M.S. Netto, D. Allasia, G.L. Dotto, Utilization of Pacara Earpod tree (Enterolobium contortisilquum) and Ironwood (Caesalpinia leiostachya) seeds as low-cost biosorbents for removal of basic fuchsine, Environ. Sci. Pollut. Res. 27 (2020) 33307–33320.
[28] R.A. Teixeira, E.C. Lima, A.D. Benetti, P.S. Thue, M.R. Cunha, N.F.G.M. Cimirro, F. Sher, M.H. Dehghani, G.S. dos Reis, G.L. Dotto, Preparation of hybrids of wood sawdust with 3-aminopropyl-triethoxysilane. Application as an adsorbent to remove Reactive Blue 4 dye from wastewater effluents, J. Taiwan Inst. Chem. Eng. 125 (2021) 141–152.
[29] M. Thommes, K. Kaneko, A.V. Neimark, J.P. Olivier, F. Rodriguez-Reinoso, J. Rouquerol, K.S.W. Sing, Physisorption of gases, with special reference to the evaluation of the surface area and pore size distribution (IUPAC Technical Report), Pure Appl. Chem. 87 (2015) 1051–1069.
[30] G.S. dos Reis, S.H. Larsson, M. Thyrel, T.N. Pham, E.C. Lima, H.P. de Oliveira, G. L. Dotto, Preparation and application of efficient biobased carbon adsorbents prepared from spruce bark residues for efficient removal of reactive dyes and colors from synthetic effluents, Coatings 11 (7) (2021) 772.
[31] J. Wang and S. Kaskel, KOH activation of carbon-based materials for energy storage, J. Mater. Chem., 45, 23710,
[32] Y. Ma, Comparison of activated carbons prepared from wheat straw via ZnCl2 and KOH activation, Waste Biomass Valoriz. 8 (2017) 549–559.
[33] A. Khelfa, G. Finqueneisel, M. Auber, J.V. Weber, Influence of some minerals on the cellulose thermal degradation mechanisms: thermogravimetric and pyrolysis-mass spectrometry studies, J. Therm. Anal. Calorim. 92 (2018) 795–799.
[34] D. Domvoglou, R. Ibbett, F. Wortmann, J. Taylor, Controlled thermo-catalytic modification of regenerated cellulosic fibres using magnesium chloride Lewis acid, Cellulose 16 (2009) 1075–1087.
[35] C. Li, G. Ji, Y. Qu, M. Irfan, K. Zhu, X. Wang, A. Li, Influencing mechanism of zinc mineral contamination on pyrolysis kinetic and product characteristics of corn biomass, J. Environ. Manag. 281 (2021), 111837.
[36] Q. Huang, G. Lu, J. Wang, J. Yu, Thermal decomposition mechanisms of MgCl2·6H2O and MgCl2·H2O, J. Anal. Appl. Pyrol. 91 (2011) 159–164.
[37] Z. Xu, Z. Yuan, D. Zhang, W. Chen, Y. Huang, T. Zhang, D. Tian, H. Deng, Y. Zhou, Z. Sun, Highly mesoporous activated carbon synthesized by pyrolysis of waste polyester textiles and MgCl2: Physiochemical characteristics and pore-forming mechanism, J. Clean. Prod. 192 (2018) 453–461.
[38] W.-J. Liu, H. Jiang, K. Tian, Y.-W. Ding, H.-Q. Yu, Mesoporous carbon stabilized MgO nanoparticles synthesized by pyrolysis of $MgCl_2$ preloaded waste biomass for highly efficient CO_2 capture, Environ. Sci. Technol. 47 (2013) 9397–9403.
[39] G.S. dos Reis, M. Adebayo, S.T. Pascal, C.H. Sampaio, E.C. Lima, S.L.P. Dias, I.A. S. De Brum, F. Pavan, Removal of phenolic compounds from aqueous solutions using sludge-Based activated carbons prepared by conventional heating and microwave-assisted pyrolysis, Water Air Soil Pollut. 228 (2017) 1–17.
[40] G.S. dos Reis, M.K.B. Mahbub, M. Wilhelm, C.H. Sampaio, E.C. Lima, C. Saucier, S. L.P. Dias, Activated carbon from sewage sludge for removal of sodium diclofenac and nimesulide from aqueous solutions, Korean J. Chem. Eng. 33 (2016) 3149–3161.
[41] G.S. dos Reis, R.A.P. Lima, S.H. Larsson, C.M. Subramaniyam, V.M. Dinh, M. Thyrel, H.P. de Oliveira, Flexible supercapacitors of biomass-based activated carbon-polypyrrole on eggshell membranes, J. Environ. Chem. Eng. 9 (2021), 106155.
[42] Y. Li, X. Zhang, R. Yang, G. Li, C. Hu, The role of H3PO4 in the preparation of activated carbon from NaOH-treated rice husk residue, RSC Adv. 5 (2015) 32626–32636.
[43] A.M. de Yuso, M. De Fina, C. Nita, P. Fioux, J. Parmentier, C.M. Ghimbeu, Synthesis of sulfur-doped porous carbons by soft and hard templating processes for CO_2 and H2 adsorption, Microporous Mesoporous Mater. 243 (2017) 135e146.
[44] G.S. dos Reis, E.C. Lima, C.H. Sampaio, F.S. Rodembusch, C.O. Petter, B. G. Cazacliu, G.L. Dotto, G.E.N. Hidalgo, Novel kaolin/ polysiloxane based organic-inorganic hybrid materials: sol-gel synthesis, characterisation, and photocatalytic properties. J. Solid State Chem. 260 (2018) (2018) 106–116.
[45] P. Kim, S. Agnihotri, Application of water-activated carbon isotherm models to water adsorption isotherms of single-walled carbon nanotubes, J. Colloid Int. Sci. 325 (2008) 64–73.
[46] D.T. Nguyen, H.N. Tran, R.S. Juang, N.D. Dat, F. Tomul, A. Ivanets, S.H. Woo, A. Hosseini-Bandegharaei, V.P. Nguyen, H.P. Chao, Adsorption process and mechanism of acetaminophen onto commercial activated carbon, J. Environ. Chem. Eng. 8 (2020), 104408.
[47] C. Saucier, P. Karthickeyan, V. Ranjithkumar, E.C. Lima, G.S. dos Reis, I.A.S. de Brum, Efficient removal of amoxicillin and paracetamol from aqueous solutions using magnetic-activated carbon, Environ. Sci. Pollut. Res. 24 (2017) 5918–5932.
[48] L. Spessato, L.C. Bedin, A.L. Cazetta, I.P.A.F. Sousa, V.A. Duarte, L.H.S. Crespo, M. C. Silva, R.M. Pontes, V.C. Almeida, KOH-super activated carbon from biomass waste: insights into the paracetamol adsorption mechanism and thermal regeneration cycles, J. Hazard. Mater. 371 (2019) 499–505.
[49] I. Cabrita, B. Ruiz, A.S. Mestre, I.M. Fonseca, A.P. Carvalho, C.O. Ania, Removal of an analgesic using activated carbons prepared from urban and industrial residues, Chem. Eng. J. 163 (2010) 249–255.
[50] O. Oginni, K. Singh, G. Oporto, B. Dawson-Andoh, L. McDonald, E. Sabolsky, Effect of one-step and two-step H3PO4 activation on activated carbon characteristics, Bioresour. Technol. Rep. 8 (2019), 100307.
[51] A. Geczo, D.A. Giannakoudakis, K. Triantafyllidis, M.R. Elshaer, E. Rodríguez-Aguado, S. Bashkova, Mechanistic insights into acetaminophen removal on cashew nutshell biomass-derived activated carbons, Environ. Sci. Pollut. Res. 28 (2021) 58969–58982.
[52] C.M. Grisales-Cifuentes, E.A.S. Galvis, J. Porras, E. Florez, R.A. Torres-Palma, N. Acelas, Kinetics, isotherms, the effect of structure, and computational analysis during the removal of three representative pharmaceuticals from water by adsorption using biochar obtained from oil palm fiber, Bioresour. Technol. 326 (2021), 124753.